Journal of Alloys and Compounds 813 (2020) 152202

Contents lists available at ScienceDirect

Journal of Alloys and Compounds

journal homepage: http://www.elsevier.com/locate/jalcom

Versatile use of ZnO interlayer in hybrid solar cells for self-powered near infra-red photo-detecting application

Jun Young Kim [a, 1], Premkumar Vincent [b, 1], Jaewon Jang [b], Min Seok Jang [c], Muhan Choi [b], Jin-Hyuk Bae [b, *], Changhee Lee [d, **], Hyeok Kim [e, ***]

[a] Department of Semiconductor Engineering, Engineering Research Institute (ERI), Gyeongsang National University, 501Jinjudaero, Jinju, Gyeongnam, 52828, Republic of Korea
[b] School of Electronics Engineering, Kyungpook National University, 80 Daehakro, Bukgu, Daegu, 702-701, Republic of Korea
[c] School of Electrical Engineering, Korea Advanced Institute of Science and Technology (KAIST), 291 Daehak-Ro, Yuseong-Gu, Daejeon, 34131, Republic of Korea
[d] Department of Electrical and Computer Engineering, Inter-University Semiconductor Research Center, Seoul National University, 1 Gwanak-ro, Gwanak-gu, Seoul, 08826, Republic of Korea
[e] Department of Electrical and Computer Engineering, University of Seoul, 163 Seoulsiripdaero, Dongdaemun-gu, Seoul, 02504, Republic of Korea

ARTICLE INFO

Article history:
Received 27 May 2019
Received in revised form
6 September 2019
Accepted 7 September 2019
Available online 9 September 2019

Keywords:
Hybrid solar cells
Optical spacer
Near-infrared organic-inorganic absorber
Optical modeling

ABSTRACT

We investigate the possibility of shifting the absorption peak of the hybrid solar cell into the red to near infra-red (NIR) region using a ZnO optical spacer. Poly[2,6-(4,4-bis-(2-ethylhexyl)-4H-cyclopenta [2,1-b; 3,4-b′]dithiophene)-alt-4,7(2,1,3-benzothiadiazole)] (PCPDTBT) exhibits a 700 nm wavelength peak absorption and is a low-bandgap polymer. Zinc oxide (ZnO) was used as an n-type semiconducting electron acceptor. The efficiency was enhanced by introducing a ZnO optical spacer layer. A finite-difference time-domain simulation was performed with the aim to extract the largest simulated short-circuit current density from the hybrid photovoltaic cell structure. Via the simulation, we also tuned the ZnO thickness to make the solar cell sensitive to the NIR wavelengths and thus obtained the optimal structures for various active layer thicknesses suitable for NIR absorption applications. This study aims to demonstrate the applicability of the PCPDTBT:ZnO hybrid solar cell as a multi-functional NIR absorber cum solar cell which has potential applications in energy harvesting window coating, NIR photodetector, and tandem solar subcell through the use of a ZnO optical layer to control the light-induced electric field distribution inside the device structure.

1. Introduction

The harvesting of solar energy to satisfy future energy requirements is an inevitable advancement. Solar farms are increasingly built to replace non-renewable energy sources [1,2]. Silicon solar cells are more common as the manufacturing of efficient silicon-based solar cells has been mastered over decades of research. In spite of their success, the high fabrication cost and inflexibility of the solar cells restrict their implementation in modern electronic devices. The high absorption coefficients of conjugated polymers allow the optimal solar absorption to be achieved with nanometer-thick layers. The low-cost fabrication, bandgap tenability, and ability to stack the solar cells in a tandem structure make thin-film solar cells a viable alternative to silicon solar cells for many applications. The combined characteristics of the organic and inorganic semiconductors are implemented into the hybrid solar cells [3–7]. They can exhibit the good charge-transfer characteristics of inorganic semiconductors and the easy processing and tunability of organic semiconductors. We studied a hybrid solar cell consisting of ZnO nanoparticles dispersed in a poly [2,6-(4,4-bis-(2-ethylhexyl)-4H-cyclopenta [2,1-b; 3,4-b′]dithiophene)-alt-4,7(2,1,3-benzothiadiazole)] (PCPDTBT) polymer matrix [8,9]. It has an energy bandgap of 1.46 eV, with the highest absorption around the near-infrared (NIR) spectrum, i.e., the wavelength range of 700–750 nm. ZnO nanoparticles are low-cost, eco-

* Corresponding author.
** Corresponding author.
*** Corresponding author.
E-mail addresses: jhbae@ee.knu.ac.kr (J.-H. Bae), chlee7@snu.ac.kr (C. Lee), hyeok.kim@uos.ac.kr (H. Kim).
[1] These authors contributed equally to this work.

https://doi.org/10.1016/j.jallcom.2019.152202
0925-8388/

friendly, n-type semiconductors that are used as the electron acceptor in BHJs [10–15]. The high charge mobility of inorganic semiconductors aids the efficient collection of electrons at the electrode. The BHJ consists of interpenetrating networks of ZnO nanoparticles in the polymer matrix. This is important as the exciton diffusion length is small in conjugated polymers. In the case of poor miscibility of the donor and acceptor molecules, the BHJ is susceptible to burn-in degradation [16]. This leads to the aggregation of one of these molecules. Aggregated molecules impact the interface charge-separation efficiency negatively. Park et al. demonstrated that 2-(2-ethylhexyl)-1,3-dioxo-2,3-dihydro-1H-benzo[de]isoquinoline-6,7-dicarboxylic acid (BQ) can be utilized to stabilize the ZnO nanoparticle, and consequently, the efficiency of the hybrid solar cell can be considerably increased [17].

In this study, by moderating the thickness of the ZnO optical spacer layer, the electromagnetic field produced by the illumination light source was concentrated into the BHJ absorption layer of the photovoltaic cell. This improved the power conversion efficiency (PCE) of the hybrid solar cell. Gilot et al. observed that the PCE of a solar cell could be augmented by a ZnO optical spacer layer [18]. Their study linked the alteration of the electric field distribution to the ZnO optical spacer layer's thickness. Our aim was to optimize the optical spacer layer through simulation to maximize the simulated short-circuit current density ($J_{sc,sim}$). The $J_{sc,sim}$ is obtained when every photo absorbed in the BHJ of the photovoltaic cell is converted to an extractable electron. In other words, $J_{sc,sim}$ is obtainable when the internal quantum efficiency (IQE) of the photovoltaic cell would be 100%. We simulated the electromagnetic field distribution in the photovoltaic cell using 2D finite difference time domain (FDTD) method. By controlling the thickness of ZnO layer, the electric field intensity concentrated within the BHJ layer was maximized, such that the optimized device structure would output the largest simulated short-circuit current density ($J_{sc,max}$). Additionally, impedance spectroscopy was performed to investigate the internal resistance of the photovoltaic cell [19,20].

Solution-processed NIR photodetectors are required in diverse applications, such as proximity sensors, medical infrared thermography, remote sensing, and thermal cameras [21–23]. The most common way to design NIR detectors is by using photon upconversion. Hybrid nanocrystals with organic molecule ligands, such as PbSe and CdSe nanocrystals combined with diphenylanthracene and rubrene as emitter ligands, absorb NIR wavelengths and re-emit visible light. This re-emitted light can be absorbed by the solar cell or a photodetector to increase the output current [24,25]. This method requires precise nanocrystal size tuning and an optimized capping layer to maintain stability. Additional upconversion layers increase the complexity of the device design. This can be overcome by using low-bandgap conjugated polymers that have a high absorption coefficient in the NIR region. Several reported low-bandgap polymers have their absorption curve in the NIR wavelength region [26–32]. Herein, we report a new polymer:ZnO nanoparticle hybrid BHJ that can be applied as a solar cell and NIR absorber. The optimized device structure was modeled to be sensitive to wavelengths ranging from 600 to 900 nm, as per the NIR spectrum provided by LIU780A (780 nm Infrared (IR) LED from Thor Labs) spectrum. The addition of ZnO optical spacer shifted the absorption peak into the NIR region. This showed that it was efficient to employ an optical spacer layer to control the absorption range, thus having promise for other NIR absorbing applications.

2. Methodology

2.1. Experimental procedure

Solution process: The PCPDTBT polymer was obtained from 1-materials while the PEDOT:PSS (CLEVIOSTM P VP Al 4083) was used as bought from CLEVIOS. ZnO nanoparticles were synthesized from potassium hydroxide (KOH), oleic acid, and zinc acetate dihydrate bought from Duksan Pharmaceutical Co., Inc, and Sigma–Aldrich (for oleic acid and zinc acetate dehydrate), respectively. The synthesis process is explained in the literature [17,33]. The ZnO nanoparticles were stabilized using the BQ surfactant added at a concentration of 3% by weight. PCPDTBT:ZnO were mixed with a weight ratio of 1:6 in chlorobenzene. The patterned indium tin oxide (ITO) substrates were sequentially cleaned using isopropyl alcohol and deionized water for 15 min each in an ultrasonic bath. The sheet resistance of the ITO substrates was 15 Ωsq^{-1}. The substrates were cleaned and then dried in an oven set to 150 °C temperature for 2 h. A 40-nm-thick PEDOT:PSS layer was spin-coated and annealed at 150 °C for 1 h. Then, the PCPDTBT:ZnO blend solution was spin-coated at 600 rpm for 60 s. The resulting BHJ layer was approximately 70 nm thick. Next, ZnO nanoparticle solution was spin-coated at 2000 rpm for 60 s to form 30 nm thick Then 100 nm of Al was evaporated under approximately 10^{-6} Torr pressure. The active area of the photovoltaic cell was 1.96 mm^2. A 300-W solar simulator (Newport 91160A, AM 1.5G with a KG 5 filter) and a Keithley 237 sourcemeter were used to measure the dark and under light (10–100 mW cm^{-2}) photocurrent-voltage characteristics. The impedance was measured in a broad frequency range (1000 Hz–10 MHz) using an impedance analyzer (HP-4192A). Ultraviolet–visible absorption spectra were obtained with a Beckman DU-70 spectrophotometer.

2.2. Optical simulation procedure

Lumerical, FDTD Solutions software was utilized in order to compute $J_{sc,sim}$ by 2D FDTD method. Since it is a planar structure, 2D FDTD was sufficient to simulate the light absorbed in the device. The distribution of the light's electromagnetic field in the solar cell could be numerically simulated using the FDTD method. The simulated structure is shown in Fig. 1. Each layer of the solar cell was stacked along the y-axis. The device was meshed with sufficient fineness that the extracted $J_{sc,sim}$ did not change with an increase in the mesh density. Perfectly matched layers were applied along with the solar cell layer stacking axis in order to confine the simulation region, and periodic boundaries were applied in the perpendicular axis. A continuous-wave (CW) normalized plane wave source was incident perpendicularly on to the ITO electrode along the forward y-axis. The source light wavelength was set from 300 nm to 900 nm in order to simulate within the absorption range

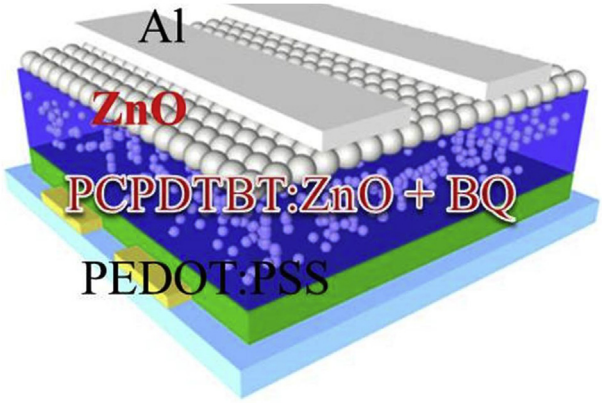

Fig. 1. The hybrid solar cell device layout with a ZnO optical spacer layer (ITO/PEDOT:PSS/PCPDTBT:ZnO + BQ/ZnO/Al).

of the active layer of the solar cell. CW-normalization provided the impulse response of the system. In order to calculate the power absorbed by the active layer from the solar spectrum, the CW-normalized output was multiplied with the solar spectrum. If the simulation were to be repeated under a different arbitrary source spectrum, it is possible to multiply the require spectrum with the CW-normalized output to obtain the power absorbed. To identify the optimal structure of the solar cell with a 70-nm-thick active layer under solar illumination, we evaluated and compared $J_{sc,sim}$ of the devices with ZnO layer thicknesses controlled from 20 nm to 50 nm with 1 nm increment. Other simulation conditions were similar to our previously published methodology [34,35]. To investigate the operation of the proposed device as a NIR absorber, a LIU780A IR LED spectrum was used to find the optimal device structure. The active layer was moderated from a start thickness of 50 nm and an end thickness of 100 nm with an increment of 10 nm thickness per simulation. For each hybrid BHJ layer thickness, the ZnO optical spacer thickness was optimized such that the responsivity of the device was maximized.

3. Results and discussion

The morphology of the BHJ layer was controlled using the BQ stabilizing agent. Fig. 2 shows the short-circuit current density vs. voltage curve. The hybrid photovoltaic cell structure with the ZnO layer was observed to have a higher fill factor (FF) and short-circuit current density (J_{sc}) than the structure without the ZnO layer. The J_{sc}, open-circuit voltage (V_{oc}), FF, and PCE of the photovoltaic cell lacking an optical spacer layer were 2.84 mA cm^{-2}, 0.59 V, 37.19%, and 0.65%, respectively, whereas the structure designed with a 30 nm thick ZnO optical spacer layer exhibited J_{sc}, V_{oc}, FF, and PCE values of 7.86 mA cm^{-2}, 0.61 V, 45.38%, and 2.25%, respectively. The addition of the ZnO optical spacer layer improved the PCE from 0.65% to 2.25%. The improvement in the PCE was attributed to the shift in the concentration of the electric field intensity from the adjacent layer into the active layer. Since light is an EM wave, the refraction, diffraction, reflection off the back electrode, etc. cause them to interfere constructively and destructively. This results in hot and cold spots of intensity of certain wavelengths of light inside the active layer of the solar cell. By controlling the thickness of the optical spacer, the intensity of specific wavelengths that would be concentrated inside the active layer could be controlled. The total number of photons absorbed is provided by the equation,

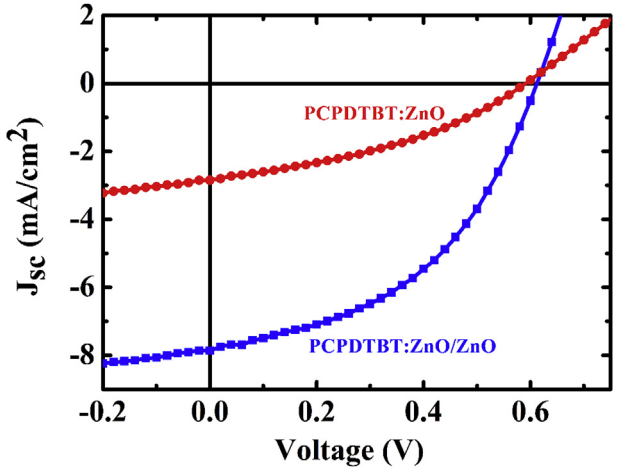

Fig. 2. Current density vs. voltage graph. The short-circuit current density of the solar cell increases from 2.84 to 7.86 mA cm^{-2} because of the addition of a ZnO optical spacer layer.

$$generation\_rate, g = \frac{-0.5|E|^2 img(\varepsilon)}{\hbar} \quad (1)$$

where E is the electric field intensity of light, img(ε) is the extinction coefficient, and ħ is the reduced plank's constant. Generation rate provides the number of electron-hole pair that are formed due to the energy absorbed from incident light. Since we assume 100% IQE, each photon absorbed leads to exactly 1 exciton pair. Due to this, the total number of photons absorbed = generation rate, g. From the generation rate, the simulated short-circuit current density can be calculated using the formula,

$$J_{sc,\,sim} = \frac{e*g}{\text{Area of the device}} \left(A/m^2\right) \quad (2)$$

As shown in Fig. 3(a)–(b), the observed normalized electric field intensity distribution was due to the interaction of light with the different photovoltaic device's layers. An FDTD simulation was performed to identify the optimal structure that provided the maximum $J_{sc,sim}$ for a solar cell having a 70 nm thick active layer. Under solar illumination, a $J_{sc,max}$ of 11.55 mA cm^{-2} was observed when the ZnO layer thickness was 38 nm. Comparatively, the $J_{sc,sim}$ obtained for the solar cell structure without the ZnO layer was 7.75 mA cm^{-2}. Because the ZnO layer also served as an electron-transport layer [36–39], it improved the charge extraction towards the Al electrode. To analyze this, impedance spectroscopy was used to characterize the internal resistance of the solar cell. Fig. 4(a) presents the Cole-Cole plot of the real part of the

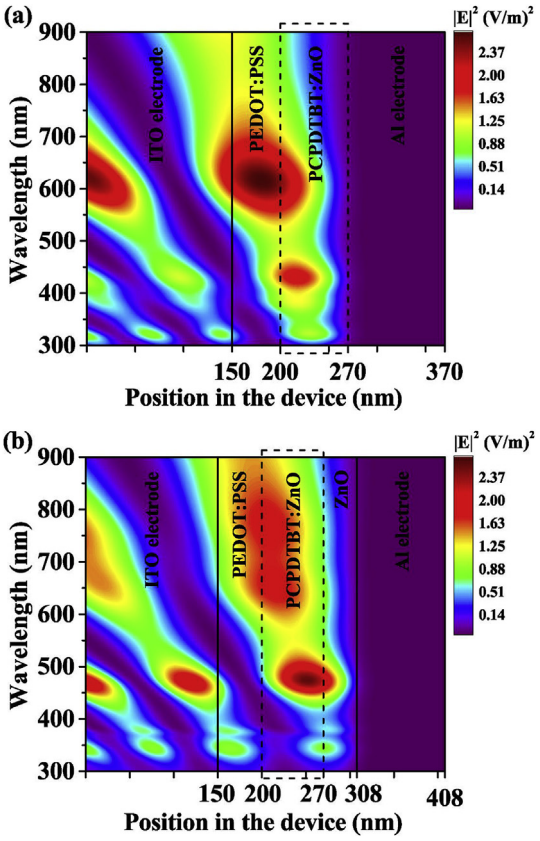

Fig. 3. The wavelength-dependent distributions of normalized electric field intensity inside the solar cell structures without (a) and with (b) a ZnO optical spacer layer. The optical spacer layer helps to shift the electric-field concentration inside the active layer. The BHJ active layer can thus absorb the higher concentration of photons. This improved the J_{sc} output from the solar cell.

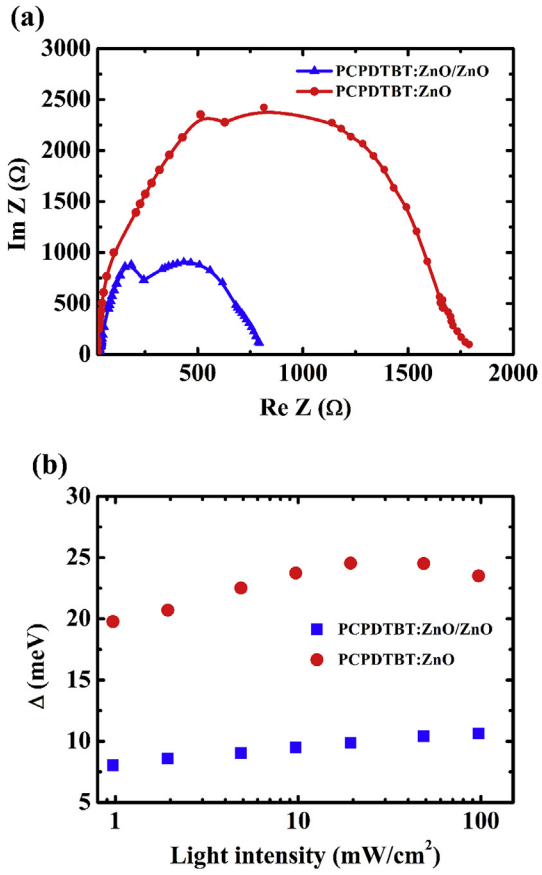

Fig. 4. (a) Cole-Cole plot of the impedance spectra. (b) The activation energy for the photovoltaic cell structures with and without the optical spacer layer. The ZnO layer also acts as an electron transport layer, reducing the internal resistance of the solar cell and aiding in efficient charge transfer to the electrodes.

impedance versus the imaginary part of the impedance of the solar cell. The impedance of the devices can be modeled as a combination of the resistance and capacitance values [33,40,41].

$$Z^* = R_C + \frac{R_J}{1 + (i\omega C R_J)^{1-\alpha}} \quad (3)$$

where C is the capacitance, α is the Cole-Cole parameter, R_C is the contact resistance, and R_J is the junction resistance, which are related to the series resistance of ITO, and interfaces between the PCPDTBT:ZnO layer and the ZnO optical spacer layer, respectively. As a result, R_C values in the high-frequency range are nearly the same for all devices (10–20Ω). However, for the low-frequency range, the junction resistance of the device without ZnO optical spacer higher R_J (~1600 Ω) than those of with the device without ZnO optical spacer (~600 Ω). These results indicate that, for the device with ZnO as an optical spacer, the charge transport property characterizing PCPDTBT:ZnO hybrid system and the charge carrier transport layers is superior to that of the device without ZnO as an optical spacer. As a results, we attribute the two semicircles in the impedance graph to the impedance associated with the active layer's charge transport mechanism, and the impedance for charge transfer to the electrodes. Fig. 4(b) shows that the activation energy was lower for the solar cell structure aided by the ZnO optical spacer layer, indicating that charge transfer was more efficient with an optical spacer layer. This also showed that the ZnO layer acts as a good optical spacer layer and also as a transport layer, thus,

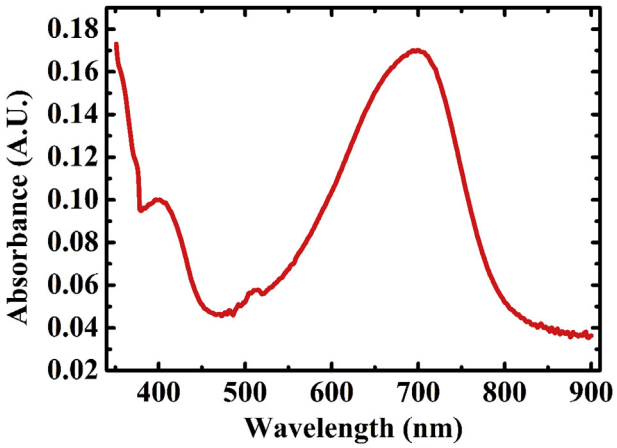

Fig. 5. Absorbance spectra of PCPDTBT:ZnO, showing an absorption peak in the wavelength range of 600–800 nm. This is suitable for NIR absorption applications, as the peak absorption wavelength is approximately 700 nm.

improving charge extraction to the electrodes. The absorbance vs. wavelength graph is shown in Fig. 5. PCPDTBT shows good absorption within the wavelength range of 550–750 nm. The absorption peaks at the NIR wavelength of 700 nm; thus, PCPDTBT can be utilized as a red to NIR absorber. This opened up the possibility of the solar cell to also work as a NIR photodetector. For NIR absorption, the solar cell structure was tuned to predominantly absorb light with wavelengths ranging from 600 nm to 900 nm. This was achieved by tuning the ZnO layer thickness. The structure was optimized to have maximum responsivity under LIU780A NIR LED spectrum's illumination. Fig. 6(a) and (b) depicts the shift in the normalized electric field intensity, at wavelengths ranging from 600 nm to 900 nm, entering the active layer. Table 1 provides the optimized ZnO layer thickness for diverse active layer thicknesses. The absorption in the active layer was simulated for different the ZnO layer thicknesses. This was repeated for diverse active layer thicknesses. The optimized optical spacer thicknesses are provided in column 2. The $J_{sc,sim}$ under sun illumination was obtained for those optimized structures. The results show that the $J_{sc,sim}$ obtained from the structures optimized to NIR wavelengths are comparable to the $J_{sc,sim}$ of the solar cell optimized for solar illumination. The multi-functional usability of the photovoltaic cell as a solar cell and NIR photodetector is thus established. Since this solar cell structure was optimized for LIU780A NIR LED spectrum, the optimized ZnO optical spacer layer thickness may vary by a few nanometers for other NIR source spectrums. This variation was, however, not large enough to significantly alter the simulation results. To obtain the $J_{sc,sim}$ generated from the solar cell, solar illumination at wavelengths ranging from 300 nm to 900 nm was used. In the optical simulation, we assumed that the internal resistance of the solar cell does not change with the ZnO layer thickness. At these thickness combinations, the dominant absorption of the solar cell occurs at the NIR wavelengths. The responsivity of the photovoltaic cell changes with ZnO optical spacer thickness. We calculated the ideal responsivity of the photovoltaic cell by extracting it from the simulated ideal external quantum efficiency. Fig. 7 depicts that with increasing thickness of the ZnO layer, the peak of the ideal responsivity (responsivity at 100% IQE), under zero bias condition, gets red-shifted. This is due to the shift in the active layer's electric field intensity distribution. When we increased the optical spacer thickness in Fig. 7, we found that the peak of the absorption curve red-shifted according to the wavelength that was highly concentrated inside the active layer. Since the PCPDTBT:ZnO material's

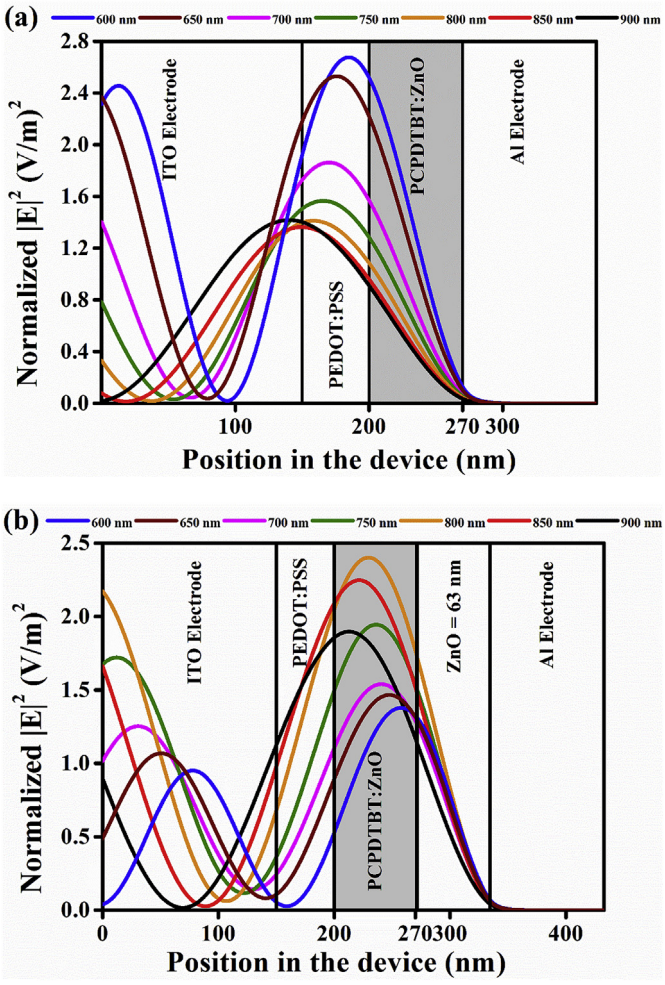

Fig. 6. The normalized electric field intensity distribution at wavelengths from 600 nm to 900 nm inside the device without (a) and with (b) a ZnO optical spacer layer. High absorption in the NIR wavelengths was achieved for a 70 nm thick active layer by setting the ZnO optical spacer layer to 63 nm for maximizing the absorption of LIU780A LED spectrum.

Table 1
Optimized ZnO layer thickness for selective NIR-wavelength absorption.

Active layer thickness (nm)	Optimized optical spacer thickness for NIR absorption (nm)	$J_{sc,sim}$ for solar illumination (mA/cm^2)
50	79	7.70
60	71	9.05
70	63	10.29
80	55	11.41
90	47	12.38
100	38	13.26

absorption characteristic is maximum at ~750 nm, during the red-shift in Fig. 7, the ideal responsivity amplitude decreases. The best absorption for a structure with an active layer thickness of 70 nm under the LIU780A NIR LED illumination was when the ZnO layer was 63 nm thick. At this optimized structure, the FWHM was 389.8 meV (165.6 nm). Kettle et al. had demonstrated PCPDTBT-ZnO based hybrid photodiode characteristics [42]. The study had stated that the active layer has one of the broadest frequency response for a hybrid photodiode. This supports our idea for utilizing it as an integrated solar cell and photodetector system. Through the proper tuning of ZnO optical spacer layer thickness,

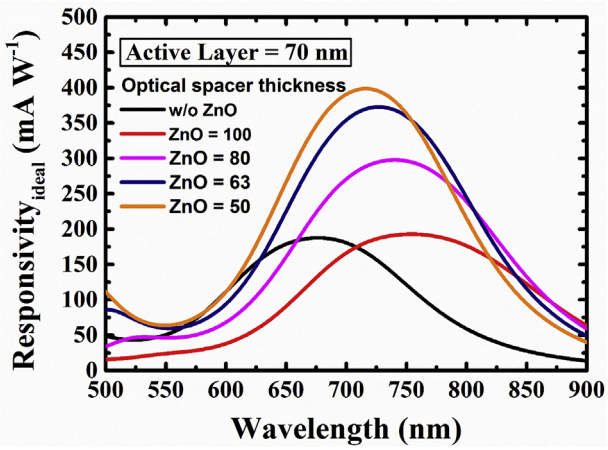

Fig. 7. Ideal responsivity (under zero bias condition) of the photovoltaic cell at different ZnO optical spacer thicknesses for the hybrid photovoltaic cell with a BHJ thickness of 70 nm. The addition of the ZnO layer red-shifted the responsivity of the solar cell. At the same time, the responsivity curve amplitude was lower, and the FWHM was also broader with the increase in ZnO layer thickness. (For interpretation of the references to colour in this figure legend, the reader is referred to the Web version of this article.)

the responsivity was maximized in the NIR spectrum region decreased in the visual light region. This absorption range can be considered similar to reported NIR photodetectors based on NIR absorbing polymers [43,44]. Our future works aim to focus on utilizing the wide absorption range of the hybrid active layer to design different applications. Since the absorption range peaks at 700 nm, it is transparent to most of the visible spectrum. This supports the usage of the hybrid solar cell as a top subcell in tandem solar cell structures. The low power requirement and self-power generation capability make it a viable option for solar cell-integrated infrared sensor arrays in electronic devices. Moreover, if the Al electrode is replaced with a suitable transparent electrode, the NIR absorber can also be used for energy harvesting windows which can block some of the sun's NIR wavelengths [21,45]. It is apt to believe our suggested NIR absorber can achieve the same.

4. Conclusion

We demonstrated a hybrid solar cell with NIR-wavelength absorption. The electric field intensity distribution was adjusted to be concentrated in the BHJ layer via the addition of a ZnO optical spacer layer. An FDTD simulation was performed to tune the optical spacer layer thickness to maximize the charge generation due to light absorption. The internal impedance was characterized via impedance spectroscopy and the decrease in the activation energy due to the inclusion of the ZnO layer was measured. As a proof of concept, the application of the hybrid solar cells as a NIR absorber was investigated. The ability to shift the responsivity of the photodetector by employing an optical spacer was discussed. The optical spacer layer thickness was tuned to concentrate the NIR wavelengths into active layers of various thicknesses. We hope that this study serves as a guide for designing low-cost multifunctional solar cell structures.

Author contributions

Conceptualization of this work was done by Changhee Lee, Jun Young Kim, and Hyeok Kim. Data curation was carried out by Premkumar Vincent, and Jun Young Kim. Formal analysis was performed by Premkumar Vincent, Jin-Hyuk Bae, and Hyeok Kim.

Investigation of the results was carried out by Premkumar Vincent, Hyeok Kim, Min Seok Jang, Jaewon Jang, and Muhan Choi. Methodology was devised by Jun Young Kim, and Premkumar Vincent. Jin-Hyuk Bae, Hyeok Kim, and Changhee Lee were in charge of the project administration. This work was carried out under the supervision of Jin-Hyuk Bae, Hyeok Kim, and Changhee Lee. All the authors shared their knowledge to the discussion and validated the manuscript.

Declarations of interest

None.

Acknowledgements

This research was supported by Basic Science Research Program through the National Research Foundation of Korea (NRF) funded by the Ministry of Science and ICT (2018R1D1A3B07049992/2018R1A2B6008815). This work was supported by MOTIE (Ministry of Trade, Industry & Energy (project number 10063474). M.S.J acknowledges the support by Creative Materials Discovery Program through the NRF funded by the Ministry of Science and ICT (NRF-2016M3D1A1900038). This work was also supproted by the NRF grant funded by the Korea government (MSIT) (No. 2017R1A4A1015565).

Appendix A. Supplementary data

Supplementary data to this article can be found online at https://doi.org/10.1016/j.jallcom.2019.152202.

References

[1] R.K. Varma, M. Salama, R. Seethapathy, C. Champion, Large-scale photovoltaic solar power integration in transmission and distribution networks, 2009, IEEE Power Energy Soc. Gen. Meet. (2009) 1–4, https://doi.org/10.1109/PES.2009.5275321.
[2] F.C. Krebs, T.D. Nielsen, J. Fyenbo, M. Wadstrøm, M.S. Pedersen, Manufacture, integration and demonstration of polymer solar cells in a lamp for the “Lighting Africa” initiative, Energy Environ. Sci. 3 (2010) 512, https://doi.org/10.1039/b918441d.
[3] W.U. Huynh, J.J. Dittmer, A.P. Alivisatos, Hybrid nanorod-polymer solar cells, Science 80– (2002), https://doi.org/10.1126/science.1069156.
[4] S. Günes, N.S. Sariciftci, Hybrid solar cells, Inorg. Chim. Acta 361 (2008) 581–588, https://doi.org/10.1016/j.ica.2007.06.042.
[5] C.-Y. Liu, Z.C. Holman, U.R. Kortshagen, Hybrid solar cells from P3HT and silicon nanocrystals, Nano Lett. 9 (2009) 449–452, https://doi.org/10.1021/nl8034338.
[6] M. Wright, A. Uddin, Organic — inorganic hybrid solar cells : a comparative review, Sol. Energy Mater. Sol. Cells 107 (2012) 87–111, https://doi.org/10.1016/j.solmat.2012.07.006.
[7] B.R. Saunders, M.L. Turner, Nanoparticle–polymer photovoltaic cells, Adv. Colloid Interface Sci. 138 (2008) 1–23. https://doi.org/10.1016/j.cis.2007.09.001.
[8] W.J.E. Beek, M.M. Wienk, R.A.J. Janssen, Efficient hybrid solar cells from zinc oxide nanoparticles and a conjugated polymer, Adv. Mater. (2004), https://doi.org/10.1002/adma.200306659.
[9] W.J.E. Beek, M.M. Wienk, R.A.J. Janssen, Hybrid solar cells from regioregular polythiophene and ZnO nanoparticles, Adv. Funct. Mater. 16 (2006) 1112–1116, https://doi.org/10.1002/adfm.200500573.
[10] Z. Zang, Efficiency enhancement of ZnO/Cu2O solar cells with well oriented and micrometer grain sized Cu2O films, Appl. Phys. Lett. 112 (2018) 42106, https://doi.org/10.1063/1.5017002.
[11] C. Li, C. Han, Y. Zhang, Z. Zang, M. Wang, X. Tang, J. Du, Enhanced photoresponse of self-powered perovskite photodetector based on ZnO nanoparticles decorated CsPbBr 3 films, Sol. Energy Mater. Sol. Cells (2017), https://doi.org/10.1016/j.solmat.2017.08.014.
[12] Z. Zang, X. Tang, Enhanced fluorescence imaging performance of hydrophobic colloidal ZnO nanoparticles by a facile method, J. Alloy. Comp. (2015), https://doi.org/10.1016/j.jallcom.2014.09.072.
[13] Z. Zang, X. Zeng, J. Du, M. Wang, X. Tang, Femtosecond laser direct writing of microholes on roughened ZnO for output power enhancement of InGaN light-emitting diodes, Opt. Lett. (2016), https://doi.org/10.1364/ol.41.003463.
[14] W.J.E. Beek, M.M. Wienk, R.A.J. Janssen, Hybrid polymer solar cells based on zinc oxide, J. Mater. Chem. 15 (2005) 2985, https://doi.org/10.1039/b501979f.
[15] W.J.E. Beek, M.M. Wienk, M. Kemerink, X. Yang, R.A.J. Janssen, Hybrid zinc oxide conjugated polymer bulk heterojunction solar cells, J. Phys. Chem. B 109 (2005) 9505–9516, https://doi.org/10.1021/jp050745x.
[16] N. Li, J.D. Perea, T. Kassar, M. Richter, T. Heumueller, G.J. Matt, Y. Hou, N.S. Güldal, H. Chen, S. Chen, S. Langner, M. Berlinghof, T. Unruh, C.J. Brabec, Abnormal strong burn-in degradation of highly efficient polymer solar cells caused by spinodal donor-acceptor demixing, Nat. Commun. 8 (2017) 14541, https://doi.org/10.1038/ncomms14541.
[17] I. Park, Y. Lim, S. Noh, D. Lee, M. Meister, J.J. Amsden, F. Laquai, C. Lee, D.Y. Yoon, Enhanced photovoltaic performance of ZnO nanoparticle/poly (phenylene vinylene) hybrid photovoltaic cells by semiconducting surfactant, Org. Electron. 12 (2011) 424–428, https://doi.org/10.1016/j.orgel.2010.12.002.
[18] J. Gilot, I. Barbu, M.M. Wienk, R.A.J. Janssen, The use of ZnO as optical spacer in polymer solar cells: theoretical and experimental study, Appl. Phys. Lett. (2007), https://doi.org/10.1063/1.2784961.
[19] R. Kern, R. Sastrawan, J. Ferber, R. Stangl, J. Luther, Modeling and interpretation of electrical impedance spectra of dye solar cells operated under open-circuit conditions, Electrochim. Acta 47 (2002) 4213–4225. https://doi.org/10.1016/S0013-4686(02)00444-9.
[20] G. Boschloo, A. Hagfeldt, Activation energy of electron transport in dye-sensitized TiO2 solar cells, J. Phys. Chem. B 109 (2005) 12093–12098, https://doi.org/10.1021/jp0513770.
[21] R.R. Lunt, V. Bulovic, Transparent, near-infrared organic photovoltaic solar cells for window and energy-scavenging applications, Appl. Phys. Lett. 98 (2011) 113305, https://doi.org/10.1063/1.3567516.
[22] J. Clark, G. Lanzani, Organic photonics for communications, Nat. Photonics 4 (2010) 438–446, https://doi.org/10.1038/nphoton.2010.160.
[23] T. Rauch, M. Boberl, S. Tedde, J. Furst, M. Kovalenko, G. Hesser, U. Lemmer, W. Heiss, O. Hayden, Near-infrared imaging with quantum dot-sensitized organic photodiodes, Nat. Photonics 3 (2009) 332–336.
[24] Z. Huang, X. Li, M. Mahboub, K.M. Hanson, V.M. Nichols, H. Le, M.L. Tang, C.J. Bardeen, Hybrid molecule-nanocrystal photon upconversion across the visible and near-infrared, Nano Lett. 15 (2015) 5552–5557, https://doi.org/10.1021/acs.nanolett.5b02130.
[25] G. Sarasqueta, K.R. Choudhury, F. So, Effect of solvent treatment on solution-processed colloidal pbse nanocrystal infrared photodetectors, Chem. Mater. 22 (2010) 3496–3501, https://doi.org/10.1021/cm1006229.
[26] L. Dou, Y. Liu, Z. Hong, G. Li, Y. Yang, Low-bandgap near-IR conjugated polymers/molecules for organic electronics, Chem. Rev. 115 (2015) 12633–12665, https://doi.org/10.1021/acs.chemrev.5b00165.
[27] M.L. Keshtov, S.A. Kuklin, N.A. Radychev, A.Y. Nikolaev, I.E. Ostapov, M.M. Krayushkin, I.O. Konstantinov, E.N. Koukaras, A. Sharma, G.D. Sharma, New low bandgap near-IR conjugated D–A copolymers for BHJ polymer solar cell applications, Phys. Chem. Chem. Phys. 18 (2016) 8389–8400, https://doi.org/10.1039/C5CP07705B.
[28] M.L. Keshtov, S.A. Kuklin, N.A. Radychev, A.Y. Nikolaev, E.N. Koukaras, A. Sharma, G.D. Sharma, Design and synthesis of new ultra-low band gap thiadiazoloquinoxaline-based polymers for near-infrared organic photovoltaic application, RSC Adv. 6 (2016) 14893–14908, https://doi.org/10.1039/C5RA24364E.
[29] J. Peet, J.Y. Kim, N.E. Coates, W.L. Ma, D. Moses, A.J. Heeger, G.C. Bazan, Efficiency enhancement in low-bandgap polymer solar cells by processing with alkane dithiols, in: Mater. Sustain. Energy A Collect. Peer-Reviewed Res. Rev. Artic. from, Nat. Publ. Gr., 2010, https://doi.org/10.1142/9789814317665_0006.
[30] X. Wang, E. Perzon, J.L. Delgado, P. De La Cruz, F. Zhang, F. Langa, M. Andersson, O. Inganäs, Infrared photocurrent spectral response from plastic solar cell with low-band-gap polyfluorene and fullerene derivative, Appl. Phys. Lett. 85 (2004) 5081–5083, https://doi.org/10.1063/1.1825070.
[31] W. Chen, Z. Du, M. Xiao, J. Zhang, C. Yang, L. Han, X. Bao, R. Yang, High-Performance small molecule/polymer ternary organic solar cells based on a layer-by-layer process, ACS Appl. Mater. Interfaces 7 (2015) 23190–23196, https://doi.org/10.1021/acsami.5b07015.
[32] C.J. Brabec, C. Winder, N.S. Sariciftci, J.C. Hummelen, A. Dhanabalan, P.A. Van Hal, R.A.J. Janssen, A low-bandgap semiconducting polymer for photovoltaic devices and infrared emitting diodes, Adv. Funct. Mater. 12 (2002) 709–712, https://doi.org/10.1002/1616-3028(20021016)12:10<709::AID-ADFM709>3.0.CO;2-N.
[33] J.Y. Kim, J. Kim, J.J. Amsden, J. Roh, I. Park, D.Y. Yoon, H. Kim, C.H. Lee, Temperature dependence and impedance characteristics of hybrid solar cells based on poly(phenylene vinylene): ZnO nanoparticles with added surfactants, IEEE J. Photovoltaics. 7 (2017) 1031–1035, https://doi.org/10.1109/JPHOTOV.2017.2690862.
[34] P. Vincent, S.C. Shin, J.S. Goo, Y.J. You, B. Cho, S. Lee, D.W. Lee, S.R. Kwon, K.B. Chung, J.J. Lee, J.H. Bae, J.W. Shim, H. Kim, Indoor-type photovoltaics with organic solar cells through optimal design, Dyes Pigments (2018), https://doi.org/10.1016/j.dyepig.2018.06.025.
[35] P. Vincent, D.S. Song, H. Bin Kwon, D.K. Kim, J.H. Jung, J.H. Kwon, E. Choe, Y.R. Kim, H. Kim, J.H. Bae, Towards maximizing the haze effect of electrodes for high efficiency hybrid tandem solar cell, Appl. Surf. Sci. (2018), https://doi.org/10.1016/j.apsusc.2017.07.204.
[36] P. de Bruyn, D.J.D. Moet, P.W.M. Blom, A facile route to inverted polymer solar cells using a precursor based zinc oxide electron transport layer, Org. Electron. 11 (2010) 1419–1422, https://doi.org/10.1016/j.orgel.2010.06.002.

[37] J. You, C.C. Chen, L. Dou, S. Murase, H.S. Duan, S.A. Hawks, T. Xu, H.J. Son, L. Yu, G. Li, Y. Yang, Metal oxide nanoparticles as an electron-transport layer in high-performance and stable inverted polymer solar cells, Adv. Mater. 24 (2012) 5267–5272, https://doi.org/10.1002/adma.201201958.
[38] Y. Sun, J.H. Seo, C.J. Takacs, J. Seifter, A.J. Heeger, Inverted polymer solar cells integrated with a low-temperature-annealed sol-gel-derived ZnO film as an electron transport layer, Adv. Mater. 23 (2011) 1679–1683, https://doi.org/10.1002/adma.201004301.
[39] H. Kim, A.R. bin, M. Yusoff, H. Kim, H. Lee, G. Seo, J. Jang, Inverted organic photovoltaic device with a new electron transport layer, Nanoscale Res. Lett. 9 (2014) 150, https://doi.org/10.1186/1556-276X-9-150.
[40] J.V. McArdle, Corrosion inhibition of iron in acid solutions by biological siderophores, J. Electrochem. Soc. (1995), https://doi.org/10.1149/1.2048595.
[41] E. McCafferty, On the determination of distributed double-layer capacitances from Cole-Cole plots, Corros. Sci. (1997), https://doi.org/10.1016/S0010-938X(97)83345-8.
[42] J. Kettle, S.W. Chang, M. Horie, Fabrication and characterisation of hybrid photodiodes based on PCPDTBT-ZnO active layers, Microelectron. Eng. (2015), https://doi.org/10.1016/j.mee.2015.05.006.
[43] A. Pickett, A. Mohapatra, A. Laudari, S. Khanra, T. Ram, S. Patil, S. Guha, Hybrid ZnO-organic semiconductor interfaces in photodetectors: a comparison of two near-infrared donor-acceptor copolymers, Org. Electron. Physics, Mater. Appl. (2017), https://doi.org/10.1016/j.orgel.2017.03.001.
[44] X. Gong, M. Tong, Y. Xia, W. Cai, J.S. Moon, Y. Cao, G. Yu, C.L. Shieh, B. Nilsson, A.J. Heeger, High-detectivity polymer photodetectors with spectral response from 300 nm to 1450 nm, Science (80) (2009), https://doi.org/10.1126/science.1176706.
[45] Y. Zhao, G.A. Meek, B.G. Levine, R.R. Lunt, Near-infrared harvesting transparent luminescent solar concentrators, Adv. Opt. Mater. (2014), https://doi.org/10.1002/adom.201400103.